

# Influence of microstructure and architecture on oxygen permeation of $\text{La}_{(1-X)}\text{Sr}_X\text{Fe}_{(1-Y)}(\text{Ga}, \text{Ni})_Y\text{O}_{3-\delta}$ perovskite catalytic membrane reactor

E. Juste<sup>a,b</sup>, A. Julian<sup>a,b</sup>, P.-M. Geffroy<sup>a,\*</sup>, A. Vivet<sup>a,b</sup>, V. Coudert<sup>a</sup>, N. Richet<sup>b</sup>,  
C. Pirovano<sup>c</sup>, T. Chartier<sup>a</sup>, P. Del Gallo<sup>b</sup>

<sup>a</sup> CNRS-ENSCI-SPCTS, 47 Avenue Albert Thomas, 87065 Limoges, France

<sup>b</sup> Air Liquide, Centre de Recherche Claude-Delorme, 1 chemin de la porte des Loges, 78354 Jouy-en-Josas Cedex, France

<sup>c</sup> Equipe de Chimie du Solide, UCCS, Unité de Catalyse et Chimie du Solide, CNRS UMR 8181, USTL-ENSCL, BP 90 108, 59652 Villeneuve d'Ascq Cedex, France

Received 21 August 2009; received in revised form 22 October 2009; accepted 4 November 2009

Available online 28 December 2009

## Abstract

Catalytic membrane reactors (CMR) have been an economically attractive process for natural gas reforming to syngas ( $\text{H}_2 + \text{CO}$ ) since more than twenty years.

The CMR studied in this paper consists of a mixed ionic and electronic conductor dense layer ( $\text{La}_{(1-X)}\text{Sr}_X\text{Fe}_{(1-Y)}\text{Ga}_Y\text{O}_{3-\delta}$ ). High temperature X-ray diffraction analysis, from room temperature to 900 °C under air and nitrogen atmosphere, show a reversible monoclinic to rhombohedral phase transition around 300 °C, and good chemical and dimensional stabilities of  $\text{La}_{0.8}\text{Sr}_{0.2}\text{Fe}_{0.7}\text{Ga}_{0.3}\text{O}_{3-\delta}$  material.

The  $\text{La}_{0.8}\text{Sr}_{0.2}\text{Fe}_{0.7}\text{Ga}_{0.3}\text{O}_{3-\delta}$  dense layer elaborated by tape casting has been respectively coated with  $\text{La}_{0.8}\text{Sr}_{0.2}\text{Fe}_{0.7}\text{Ga}_{0.3}\text{O}_{3-\delta}$  on the air side and  $\text{La}_{0.8}\text{Sr}_{0.2}\text{Fe}_{0.7}\text{Ni}_{0.3}\text{O}_{3-\delta}$  on the inert side using screen printing. The influences of the dense membrane microstructure and of the surface exchange kinetics on the oxygen semi-permeation performances are evaluated. Small grain size, mainly below 1  $\mu\text{m}$  in the dense membrane significantly increases the oxygen flux. A porous layer of  $\text{La}_{0.8}\text{Sr}_{0.2}\text{Fe}_{0.7}\text{Ni}_{0.3}\text{O}_{3-\delta}$  or  $\text{La}_{0.8}\text{Sr}_{0.2}\text{Fe}_{0.7}\text{Ga}_{0.3}\text{O}_{3-\delta}$  on the air or inert side of the membrane increased strongly the specific oxygen semi-permeation. The impact of the porous layer is much more important than the reduction of the grain size. In this case, surface exchange kinetics are the limiting steps of oxygen permeation, and Ni-containing formulation leads to the highest flux.

© 2009 Elsevier Ltd. All rights reserved.

**Keywords:** Catalytic membrane reactor; Oxygen semi-permeation; Oxygen surface exchange; Microstructure; Ceramic membrane multilayer

## 1. Introduction

Over the last decade, the interest in catalytic membrane reactors (CMR) has increased due to the potential benefits they can offer to convert methane into synthesis gas ( $\text{H}_2$  CO mixture). Synthesis gas or syngas is used as precursor for more value-added products (polymers, chemicals, ...) and synthetic fuels [1–3]. CMR technology is based on the separation of the oxygen from air and the conversion of methane to syngas in a single reactor. The CMR technology does not need oxygen feed by cryogenic distillation, leading to lower capital investment and potential higher efficiency than conventional processes [4,5]. For an industrial development, the key parameters are

membranes lifetime and performances in terms of oxygen semi-permeation.

A dense ceramic membrane based on perovskite type oxide, with both ionic and electronic conduction properties, is the main part of the reactor. When an oxygen partial pressure gradient is applied on between their opposite surfaces of the membrane and at a temperature typically above 700 °C, an oxygen flux takes place. Pure oxygen permeates through the dense membrane from the oxygen rich (air) to the oxygen lean surface (inert gas or methane). On the oxygen lean surface, a catalyst layer can be used to favor the reactions producing syngas (partial oxidation, steam reforming).

Numerous mixed ionic and electronic oxides have been studied in recent years in view of potential use, as membrane material in CMR application. A particular attention has been brought to the group of perovskite oxides  $(\text{La}, \text{Fe})(\text{Sr}, \text{Ga})\text{O}_{3-\delta}$ , due to their excellent chemical stability in operating conditions and their oxygen semi-permeation performances.

\* Corresponding author. Tel.: +33 5 55 45 22 65; fax: +33 5 55 79 69 54.  
E-mail address: [pierre-marie.geffroy@unilim.fr](mailto:pierre-marie.geffroy@unilim.fr) (P.-M. Geffroy).

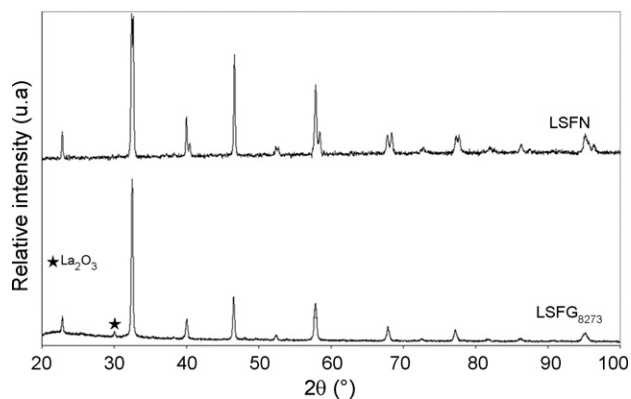


Fig. 1. XRD patterns of prepared  $\text{La}_{0.8}\text{Sr}_{0.2}\text{Fe}_{0.7}\text{Ga}_{0.3}\text{O}_{3-\delta}$  and  $\text{La}_{0.8}\text{Sr}_{0.2}\text{Fe}_{0.7}\text{Ni}_{0.3}\text{O}_{3-\delta}$  powders.

A previous work [6] concerning the influence of the cationic substitution on the membrane performances (dimensional stabilities and oxygen semi-permeation rate) has concluded that  $\text{La}_{0.7}\text{Sr}_{0.3}\text{Fe}_{0.7}\text{Ga}_{0.3}\text{O}_{3-\delta}$  and vicinity materials present a good compromise to satisfy all requirements for a CMR application.

The present study considers firstly the thermo-structural stability of the  $\text{La}_{0.8}\text{Sr}_{0.2}\text{Fe}_{0.7}\text{Ga}_{0.3}\text{O}_{3-\delta}$  material for the dense membrane. Dimensional and structural stabilities were studied by dilatometric measurements and high temperature X-rays diffraction (HT-XRD) under two oxygen partial pressures (0.21 and  $10^{-5}$  atm). In a second time, the influence of the grain size of the membrane (microstructural effect) and the deposit of a porous layer on both faces of the membrane (architectural effect) on oxygen permeation have been investigated. The  $\text{La}_{0.8}\text{Sr}_{0.2}\text{Fe}_{0.7}\text{Ga}_{0.3}\text{O}_{3-\delta}$  dense layer elaborated by tape casting has been coated by screen printing on the inert gas (Argon) and the air side with  $\text{La}_{0.8}\text{Sr}_{0.2}\text{Fe}_{0.7}\text{Ga}_{0.3}\text{O}_{3-\delta}$  or  $\text{La}_{0.8}\text{Sr}_{0.2}\text{Fe}_{0.7}\text{Ni}_{0.3}\text{O}_{3-\delta}$  thin porous layer.

## 2. Experimental procedure

### 2.1. Powder synthesis

The perovskite powders,  $\text{La}_{0.8}\text{Sr}_{0.2}\text{Fe}_{0.7}\text{Ga}_{0.3}\text{O}_{3-\delta}$  (referenced LSFG<sub>8273</sub>) and  $\text{La}_{0.8}\text{Sr}_{0.2}\text{Fe}_{0.7}\text{Ni}_{0.3}\text{O}_{3-\delta}$  (referenced LSFN<sub>8273</sub>), are synthesized by spray pyrolysis process (Pharmacie Centrale de France). The as-synthesized powders are agglomerated and exhibit a high BET surface area around  $17\text{ m}^2\text{ g}^{-1}$ . These powders were calcined at  $1000^\circ\text{C}$  during 6 h, then attrition-milled using zirconia balls media in ethanol and a dispersing agent CP213 (Cerampilote, Limoges France), in order to obtain a narrow distribution with dense particles having a mean size of  $0.3\text{ }\mu\text{m}$  for LSFG<sub>8273</sub>,  $0.2\text{ }\mu\text{m}$  for LSFN and a BET surface area of around  $10\text{ m}^2\text{ g}^{-1}$  for both.

After attrition milling, LSFG<sub>8273</sub> and LSFN<sub>8273</sub> powders were controlled by XRD analysis (Fig. 1). LSFG<sub>8273</sub> powder presented minor  $\text{La}_2\text{O}_3$  secondary phase. No impurities were detected for the  $\text{La}_{0.8}\text{Sr}_{0.2}\text{Fe}_{0.7}\text{Ni}_{0.3}\text{O}_{3-\delta}$  powder.

### 2.2. Characterizations

During the attrition-milling process step, grain size distribution was controlled with a laser granulometer (Malvern Instruments Mastersizer 2000). Densities of sintered samples were measured by the Archimede method. Microstructures were observed by Scanning Electron Microscope (SEM S-2500, Hitachi). The grain size distribution of the dense membranes was computed by image analysis software on about 1000 grains assimilated to spheres (Aphelion, ADCIS, France). Grains boundary of a polished cross-section is thermally etched  $50^\circ\text{C}$  below the sintering temperature for 12 min.

In situ high temperature X-ray diffraction (HT-XRD) was conducted on LSFG<sub>8273</sub> powder, calcined at  $1250^\circ\text{C}$  for 2 h, under air flow and nitrogen flow (Bruker D8 diffractometer with high temperature cell (HTK 1200N) equipped with a Vantec detector). The measurements were performed using  $\text{CuK}\alpha$  radiation in the  $2\theta$  range of  $20$ – $80^\circ$  with  $0.0148^\circ$  step. The heating and cooling rates, between room temperature and  $900^\circ\text{C}$ , were  $5^\circ\text{C min}^{-1}$ . At each step, the temperature was held for 15 min to establish thermal equilibrium before data acquisition. At  $900^\circ\text{C}$ , the temperature was held 10 h. During the dwell time, a X-ray pattern was collected every hour.

The expansion behaviour was measured under air and nitrogen flow. The samples are 5 mm long beam extracted from laminated membranes sintered at  $1250^\circ\text{C}$  during 2 h. Dilatometric characterizations were performed using a Thermal Mechanical Analysis (Setaram evolution) from room temperature to  $1050^\circ\text{C}$  with heating and cooling rates of  $5^\circ\text{C min}^{-1}$  or  $2^\circ\text{C min}^{-1}$  and a gas flow rate of  $30\text{ ml min}^{-1}$ .

The oxygen semi-permeation measurements were performed using a specific device described in a previous paper [6]. A 1 mm thick dense membrane, 24 mm in diameter, is sealed between two alumina tubes using a home-made Pyrex-based glass to obtain a tight system. Upon both opposite faces, gas flows (synthetic air to the bottom and argon to the upper face) are injected to impose an oxygen partial pressure gradient. Oxygen content in argon is monitored using an Yttria-stabilized Zirconia (YSZ)-oxygen sensor for temperature ranging from  $750$  to  $1000^\circ\text{C}$  by steps of 10 or  $20^\circ\text{C}$ . The oxygen semi-permeation flux was calculated using Eq. (1).

$$j_{\text{O}_2} = \frac{CD}{S} \alpha \quad (1)$$

where  $j_{\text{O}_2}$  is the oxygen semi-permeation flux through the dense membrane ( $\text{Nm}^3\text{ m}^{-2}\text{ h}^{-1}$ ),  $C$  the measured oxygen amount (ppm),  $D$  the argon carrier gas output flow rate ( $\text{m}^3\text{ h}^{-1}$ ),  $S$  the membrane effective reacting area ( $\text{m}^2$ ) ( $S = 2.83 \times 10^{-4}\text{ m}^2$ ) and  $\alpha$  the normalization volume coefficient function of the room temperature and pressure as defined in Eq. (2):

$$\alpha = \frac{P_{\text{room}} \times T_{(\text{STP})}}{P_{(\text{STP})} \times T_{\text{room}}} \quad (2)$$

where  $T_{(\text{STP})} = 298\text{ K}$  and  $P_{(\text{STP})} = 10^5\text{ Pa}$ .

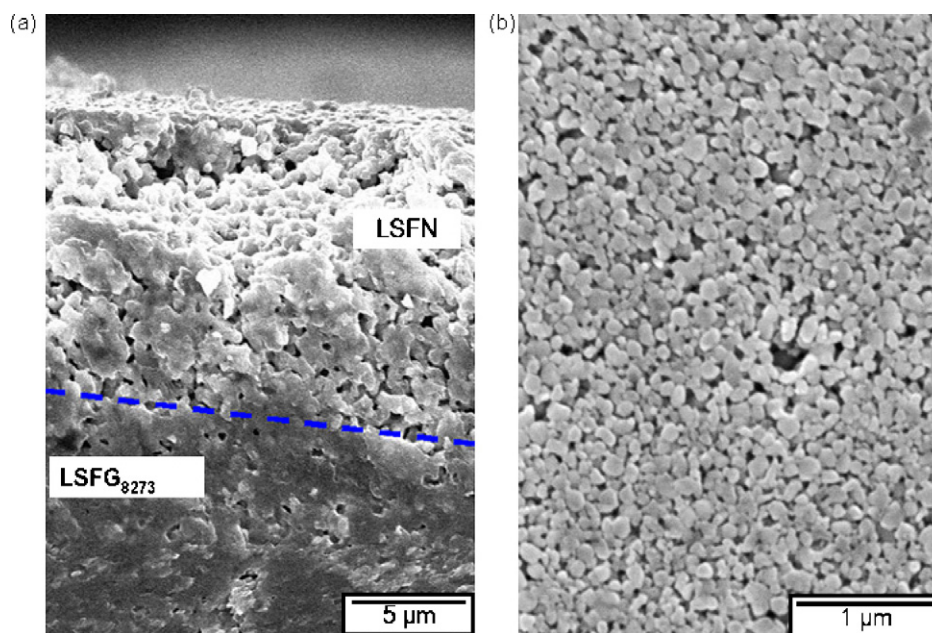


Fig. 2. SEM micrographs of LSFN/LSFG<sub>8273</sub> architecture (a) polished cross section La<sub>0.8</sub>Sr<sub>0.2</sub>Fe<sub>0.7</sub>Ga<sub>0.3</sub>O<sub>3-δ</sub> coated with a low porous (27%) layer of La<sub>0.8</sub>Sr<sub>0.2</sub>Fe<sub>0.7</sub>Ni<sub>0.3</sub>O<sub>3-δ</sub> and (b) top view of porous La<sub>0.8</sub>Sr<sub>0.2</sub>Fe<sub>0.7</sub>Ni<sub>0.3</sub>O<sub>3-δ</sub>.

### 2.3. Membranes: shaping and coating

Dense LSFG<sub>8273</sub> membranes for oxygen permeation flux measurements were shaped by tape casting. A shear-thinning slurry was prepared from LSFG<sub>8273</sub> attrition-milled powder by adding a binder (methyl methacrylate, Degalan LP51/07 Degussa), a plasticizer (dibutyl phthalate, Sigma–Aldrich) and a dispersing agent (CP 213, Cerampilote, Limoges France) in an azeotropic solvent of butanone-2 and ethanol. A cohesive and flexible green tape with a controlled thickness is obtained using a doctor blade tape casting apparatus.

The green tape was pounded into disks, which were stacked then laminated. Stacks were sintered to obtain 1 mm thick dense membranes with a relative density above 95% of theoretical density of the powder.

A LSFG<sub>8273</sub> and LSFN<sub>8273</sub> serigraphy inks is prepared from attrition-milled powders dispersed in an organic medium with the addition of rice starch as pore forming agent. A thin layer of ink is screen printed onto one side surface of the LSFG<sub>8273</sub> dense membrane and dried at room temperature. Then a heat treatment at 1100 °C during 30 min after organics removal, leads to a 10 µm thick porous layer with a porosity varying from 27 to 50% vol% depending on the concentration of pore former agent. As shown in Fig. 2 a well adherent LSFN<sub>8273</sub> porous layer is deposited on the dense LSFG<sub>8273</sub> membrane. This architecture is referenced LSFN/LSFG<sub>8273</sub> (27 vol% of porosity) or p LSFN/LSFG<sub>8273</sub> (50 vol% of porosity) in this paper.

## 3. Results and discussion

### 3.1. Dilatometric and structural behaviour

La<sub>0.8</sub>Sr<sub>0.2</sub>Fe<sub>0.7</sub>Ga<sub>0.3</sub>O<sub>3-δ</sub> materials present a singular expansion behaviour. The apparent thermal expansion coefficient

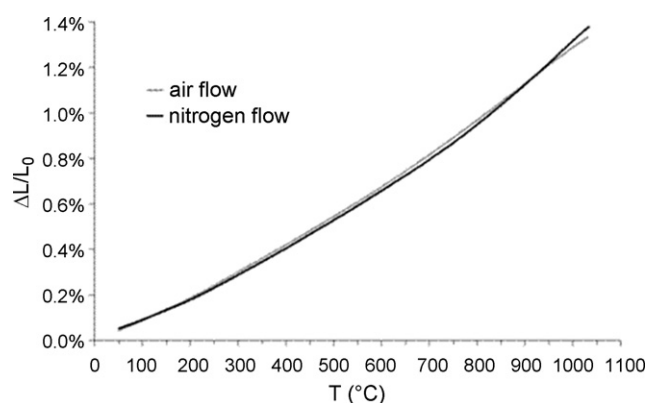


Fig. 3. Comparison of dilatometric curves of La<sub>0.8</sub>Sr<sub>0.2</sub>Fe<sub>0.7</sub>Ga<sub>0.3</sub>O<sub>3-δ</sub> perovskite under air and nitrogen flow.

(TEC) is defined as the slope of the expansion curve (Fig. 3). Below 600 °C, a classical thermal expansion, due to lattice vibrations with temperature is measured. Whereas, above 870 °C, apparent expansion coefficient increases due to cell volume expansion caused by oxygen vacancies formation in the perovskite structure [2,7]. This phenomenon is known as chemical expansion. This singular expansion behaviour has been investigated in our previous paper [6]. In case of LSFG<sub>8273</sub> material, the difference between TEC under air and under nitrogen above 870 °C is 19% (Table 1),

Table 1

Thermal expansion coefficients of La<sub>0.8</sub>Sr<sub>0.2</sub>Fe<sub>0.7</sub>Ga<sub>0.3</sub>O<sub>3-δ</sub> membrane under air and nitrogen flow.

	Atmosphere	$T < 800\text{ °C}$	$T > 800\text{ °C}$
TEC ( $\times 10^{-6}$ )	Air ( $p_{\text{O}_2} = 0.21\text{ atm}$ )	11.9	16.0
	Nitrogen ( $p_{\text{O}_2} = 5 \times 10^{-6}\text{ atm}$ )	12.3	19.0

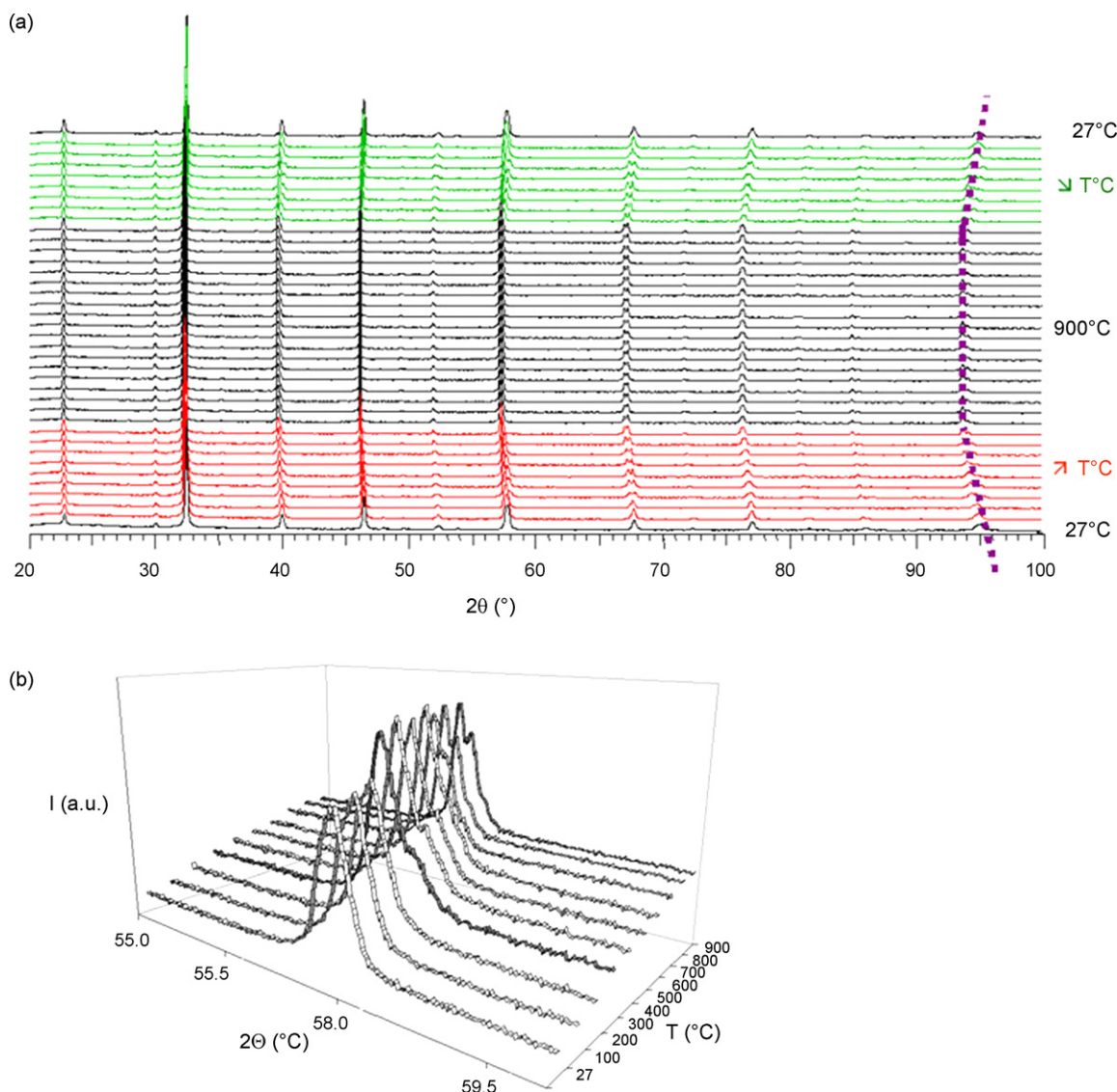


Fig. 4. Evolution (a) of XRD patterns of  $\text{La}_{0.8}\text{Sr}_{0.2}\text{Fe}_{0.7}\text{Ga}_{0.3}\text{O}_{3-\delta}$  scanned from room temperature to 900°C under air flow (b) detail during the increase temperature showing a split of a peak.

and similar CTE difference was observed for  $\text{LSFG}_{7373}$  [6] (Fig. 4).

### 3.2. XRD analysis

Fig. 5 presents the evolution of the XRD patterns of  $\text{LSFG}_{8273}$  under air and nitrogen flow with the temperature. Peaks splitting ( $2\theta$  about 40°, 58° and 67°) were observed around 300°C while the temperature is increasing under both atmospheres, suggesting a phase transition between 300 and 400°C (Fig. 5b).

Under air, XRD patterns are reversible during heating and cooling (Figs. 4 and 5). Under nitrogen flow, the phase transition occurred at about 400°C upon cooling instead of 300°C during heating. The final XRD pattern at room temperature presented a slight hysteresis (Fig. 5b). This slight difference between both atmospheres could be explained by the formation of oxygen vacancies at high temperature that cannot be withdrawn during

cooling due to the low oxygen partial pressure. TG analysis reported in a previous work [8] confirm this behaviour.

Diffraction pattern of the perovskite can be indexed in a monoclinic structure with  $P2/c$  space group from room temperature to 200–300°C. Between 200 and 300°C,  $\text{LSFG}_{8273}$  crystalline symmetry evolves from monoclinic to rhombohedral. From 300 to 900°C,  $\text{LSFG}_{8273}$  perovskite diffraction peaks could be indexed in a  $R-3c$  space group.

XRD analysis, versus temperature and  $p\text{O}_2$ , show that  $\text{LSFG}_{8273}$  has a stable structure up to 1000°C under air and nitrogen flow. The reversible evolution of the crystal cell structure can be explained by perovskite lattice distortion due to the reduction of iron cations and the creation of oxygen vacancies [8].

Some studies have shown an influence of the temperature on the crystal structure of  $\text{La}_{(1-x)}\text{Sr}_x\text{Fe}_{(1-y)}\text{Ga}_y\text{O}_{3-\delta}$ . Koutcheiko et al. [9] reported for  $\text{La}_{0.7}\text{Sr}_{0.3}\text{Fe}_{0.6}\text{Ga}_{0.4}\text{O}_3$  a phase transition from hexagonal to cubic around 600°C with an increase of the

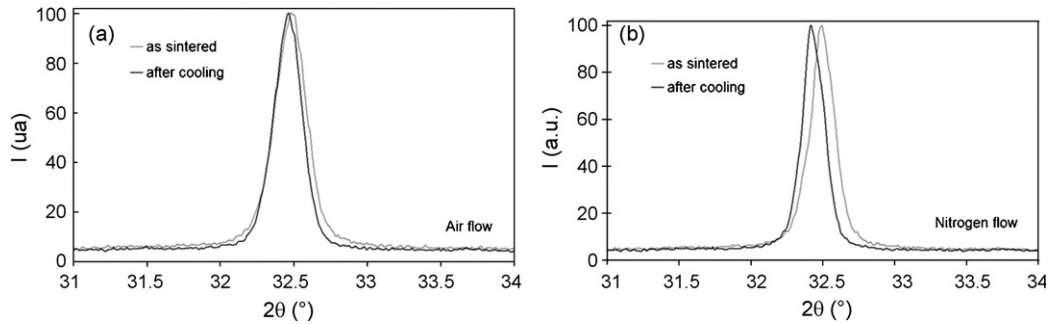


Fig. 5. Comparison at room temperature of a peak (100) of the XRD pattern of  $\text{La}_{0.8}\text{Sr}_{0.2}\text{Fe}_{0.7}\text{Ga}_{0.3}\text{O}_{3-\delta}$  after heating and cooling (a) under air, (b) under nitrogen flow.

volume. They explain this phenomenon by the reduction of Fe cations ( $\text{Fe}^{4+}$  in  $\text{Fe}^{3+}$ , or  $\text{Fe}^{3+}$  in  $\text{Fe}^{2+}$ ). McIntosh et al. [10] have observed the influence of temperature and  $p\text{O}_2$  on unit cell symmetry for  $\text{SrCo}_{0.8}\text{Fe}_{0.2}\text{O}_{3-\delta}$ . This material presents a cubic structure with a space group  $Pm\bar{3}m$  in air at room temperature. In the temperature range 300–700 °C under a nitrogen flow,  $\text{SrCo}_{0.8}\text{Fe}_{0.2}\text{O}_{3-\delta}$  evolves to orthorhombic symmetry associated with the formation of a brownmillerite structure. Between 700 and 800 °C, the cubic symmetry is restored. Wang et al. [11] have also observed for  $\text{SrCo}_{0.8}\text{Fe}_{0.2}\text{O}_{3-\delta}$ ,  $\text{Ba}_{0.5}\text{Sr}_{0.5}\text{Co}_{0.8}\text{Fe}_{0.8}\text{O}_{3-\delta}$  and  $\text{BaCo}_{0.4}\text{Fe}_{0.4}\text{Zr}_{0.2}\text{O}_{3-\delta}$  oxides a reversible variation of XRD patterns from 30 to 1000 °C with a phase transition attributed to the reduction of metal ions and the formation of oxygen vacancies [11].

Julian et al. [8] give a better understanding of the influence of the temperature on  $\text{La}_{(1-x)}\text{Sr}_x\text{Fe}_{(1-y)}\text{Ga}_y\text{O}_{3-\delta}$  structure and its thermo-mechanical properties. The Fe substitution by Ga leads to a decrease of the thermal expansion at high temperature, but also to a significant decrease of the Young modulus of  $\text{La}_{(1-x)}\text{Sr}_x\text{Fe}_{(1-y)}\text{Ga}_y\text{O}_{3-\delta}$ . Ga doping in  $\text{La}_{(1-x)}\text{Sr}_x\text{Fe}_{(1-y)}\text{Ga}_y\text{O}_{3-\delta}$  perovskite leads to local distortions of the structure and the phase change from monoclinic to rhombohedral between 200 and 300 °C. However, the phase transition has no impact on the thermal expansion coefficient of perovskite. In this respect, the Ga doping improves the thermo-mechanical properties because of the decrease of the thermal expansion coefficient and the stiffness of the perovskite.

One of the main properties of the membrane material is the oxygen semi-permeation flux. This property can be strongly impacted by the mean grain size of the dense membrane (microstructural effect) and the modification of membrane surface by the coating with a porous layer (architectural effect).

### 3.3. Oxygen permeation

#### 3.3.1. Relation between dense membrane microstructure and oxygen permeation

Numerous authors have related the relation between the microstructure of the membrane and the oxygen semi-permeation. For instance, Etchegoyen et al. [12] have reported an improvement of oxygen semi-permeation flux through a  $\text{La}_{0.6}\text{Sr}_{0.4}\text{Fe}_{0.9}\text{Ga}_{0.1}\text{O}_{3-\delta}$  dense membrane with the decrease of the mean grain size. Kharton et al. [13,14] have observed

the opposite behaviour with an increase of the oxygen semi-permeation flux when grain size increase for  $\text{LaCoO}_{3-\delta}$  and  $\text{SrCo}(\text{Fe}, \text{Cu})\text{O}_{3-\delta}$ . Similar results were obtained by Wang et al. [15] for  $\text{Ba}_{0.5}\text{Sr}_{0.5}\text{Co}_{0.8}\text{Fe}_{0.2}\text{O}_{3-\delta}$  membranes and by Martynczuk et al. [16] and Arnold et al. [17] for  $(\text{Ba}_{0.5}\text{Sr}_{0.5})(\text{Fe}_{0.8}\text{Zn}_{0.2})\text{O}_{3-\delta}$  membranes. For these last materials, the semi-permeation flux increases with the mean grain size. Hence, a general explanation cannot be given about the influence of microstructure of the membrane on oxygen semi-permeation flux, probably because many parameters can be involved to powder synthesis process, powder purity, shaping process, . . .

The influence of the microstructure of the membrane materials on the oxygen semi-permeation was investigated in this paper for three grain size distributions (Table 2). The grain size distribution was adjusted by mean of the sintering conditions (i.e. temperature and dwell time). The mean grain diameter obtained were 0.47, 0.95 and 1.70  $\mu\text{m}$  (Fig. 6).

The bulk diffusion step is usually the slowest mechanism. In this case the oxygen flux follows the Wagner theory [3] in Eq. (3):

$$J_{\text{O}_2} = \frac{RT}{16F^2L} \int_{p\text{O}_2''}^{p\text{O}_2'} \sigma_{\text{ion}} d\ln(p\text{O}_2) \quad (3)$$

Oxygen semi-permeation depends on the thickness of the membrane and oxygen partial pressure gradient through the membrane. In order to compare the materials performances, the specific oxygen semi-permeation, which does not depend on thickness of membrane, is defined by the following relationship

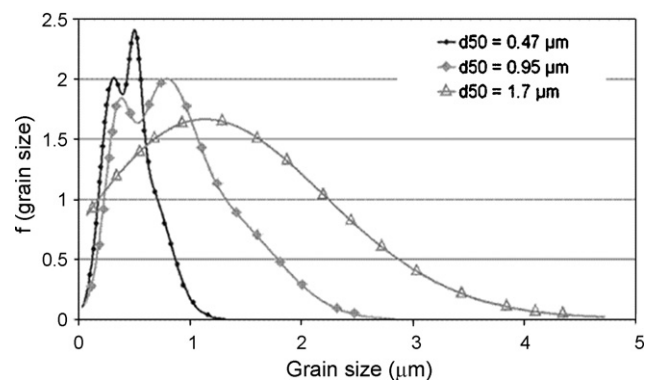
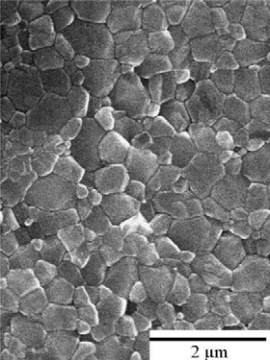
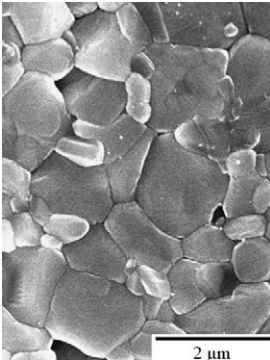
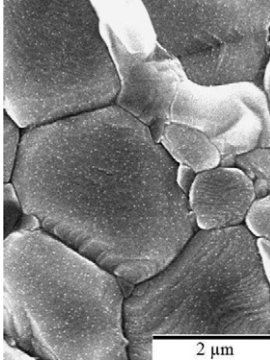


Fig. 6. Grain size distribution of LSFG8273 materials presented in Table 2.

Table 2

Sintering conditions and mean grain size of the LSFG<sub>8273</sub> membranes.

Sintering conditions	1250 °C/2 h	1350 °C/10 h	1400 °C/10 h
Relative density	99%	98%	96%
Mean grain diameter (μm)	0.47	0.95	1.70
Standard deviation grain diameter (μm)	0.31	0.56	1.07
Micrograph			

(Eq. (4)) proposed by Kharton et al. [14].

$$jO_2^* = \frac{jO_2}{\ln(pO_2'/pO_2'')} \times L \quad (4)$$

where  $pO_2'$  is the oxygen partial pressure on the oxygen rich side and  $pO_2''$  the oxygen partial pressure on oxygen poor side. The term  $\ln(pO_2'/pO_2'')$  takes into account the influence of the evolution of the oxygen partial pressure gradient with the temperature on the oxygen semi-permeation.

However, the Wagner theory is not applicable when the oxygen flux through the membrane is controlled by surface exchange kinetics. In this case, the specific oxygen semi-permeation depends on the thickness of membrane.

Fig. 7 shows the evolution of the specific oxygen semi-permeation flux with the temperature for the three microstructures. The specific oxygen flux through  $\text{La}_{0.8}\text{Sr}_{0.2}\text{Fe}_{0.7}\text{Ga}_{0.3}\text{O}_{3-\delta}$  material increases with the temperature and the decrease of the grain size. At 900 °C, the specific oxygen semi-permeation flux are respectively  $1.0 \times 10^{-5}$  and

$1.4 \times 10^{-5} \text{ ml cm}^{-1} \text{ min}^{-1}$  for membranes with a mean grain size of 1.70 and 0.95 μm. For an average grain size of 0.47 μm, the specific oxygen semi-permeation flux reaches  $2.7 \times 10^{-5} \text{ ml cm}^{-1} \text{ min}^{-1}$  at 900 °C.

Contrary to the results obtained by Kharton et al. [14,18] for different mixed conductors, grain boundaries in  $\text{La}_{0.8}\text{Sr}_{0.2}\text{Fe}_{0.7}\text{Ga}_{0.3}\text{O}_{3-\delta}$  materials do not constitute barriers for oxygen transport. The increase of specific oxygen semi-permeation flux for higher density of grain boundaries could be explained by a significant role of grain boundaries in oxygen transport. It is well known that grain boundaries contain a lot of crystalline defects, for instance oxygen vacancies that leads to a more rapid path of oxygen in the bulk of the membrane [19]. Another assumption is that the grain boundary density could improve significantly oxygen exchange kinetics on the surface of the membrane. Grain boundaries at the surface of the membrane are favored sites for oxygen adsorption from air or oxygen desorption to argon sweep gas. In other terms, a surface exchange rate-limiting mechanism may govern the oxygen transport through the dense membrane that is investigated in the next section.

### 3.3.2. Influence of the membrane thickness on oxygen permeation

When bulk diffusion mechanisms of oxygen are the limiting steps, the flux variations follow the Wagner theory: Eq. (5) [20]:

$$jO_2 = \frac{-RT}{16F^2L} \int_{\ln pO_2''}^{\ln pO_2'} \frac{\sigma_{el} \times \sigma_{ion}}{\sigma_{el} + \sigma_{ion}} d \ln(pO_2) \quad (5)$$

where  $R$  is the ideal gas constant;  $T$  the temperature;  $F$  the Faraday constant,  $L$  the membrane thickness, and  $\sigma_{el}$  and  $\sigma_{ion}$  are the electronic and ionic conductivity, respectively.

The oxygen flux through LSFG<sub>8273</sub> dense membranes with a mean grain size of 0.47 μm were measured for two thicknesses: 1.0 and 1.7 mm. The evolution of the specific oxygen flux between 750 and 1000 °C with the thickness (Fig. 8) suggests that the bulk oxygen diffusion is not the rate-controlling

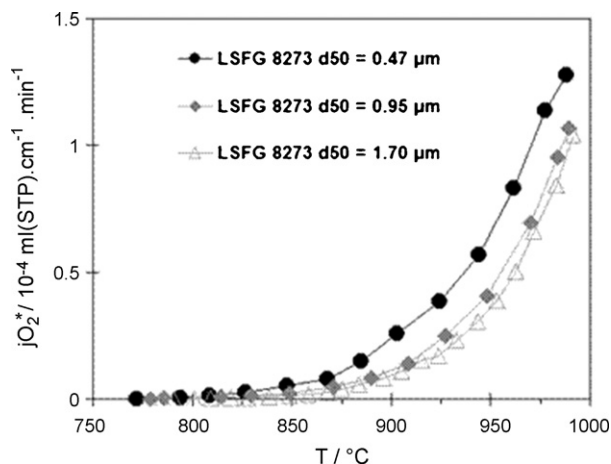


Fig. 7. Specific oxygen semi-permeation flux through  $\text{La}_{0.8}\text{Sr}_{0.2}\text{Fe}_{0.7}\text{Ga}_{0.3}\text{O}_{3-\delta}$  dense membrane for three mean grain sizes.

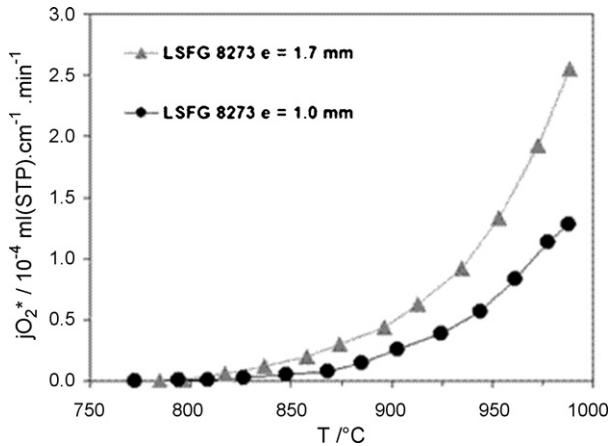


Fig. 8. Specific oxygen semi-permeation flux through  $\text{La}_{0.8}\text{Sr}_{0.2}\text{Fe}_{0.7}\text{Ga}_{0.3}\text{O}_{3-\delta}$  membrane with different thicknesses.

mechanism. In this respect, we can assume that oxygen surface exchanges for both surfaces are the rate-controlling mechanisms of oxygen semi-permeation [21,22].

### 3.3.3. Influence of surface exchanges kinetics on oxygen permeation

As bulk diffusion is not the limiting step of the diffusion, surface exchanges kinetics are key parameters to increase the oxygen flux. Two ways are proposed to improve surface exchange kinetics:

- (1) Increase the surface by coating the membrane with a porous layer. This way has been investigated in previous papers [23,24].

- (2) Add catalysts of respectively oxygen dissociation on the oxygen rich side and of the conversion reactions on the oxygen poor side.

On an experimental point of view it is difficult to separate those two contributions. We have decided to use a porous coating of a catalyst material. Moreover, the porous layer can also act as a support for mechanical resistance, especially if thin dense membrane is required.

In this respect, the  $\text{La}_{0.8}\text{Sr}_{0.2}\text{Fe}_{0.7}\text{Ga}_{0.3}\text{O}_{3-\delta}$  dense membrane has been coated with  $\text{La}_{0.8}\text{Sr}_{0.2}\text{Fe}_{0.7}\text{Ga}_{0.3}\text{O}_{3-\delta}$  (p LSFG) or  $\text{La}_{0.8}\text{Sr}_{0.2}\text{Fe}_{0.7}\text{Ni}_{0.3}\text{O}_{3-\delta}$  (p LSFN) thin porous layer by screen printing respectively on the oxygen rich and oxygen poor sides. Ni is well-known as catalyst for methane conversion reactions (POM, SMR, ...).

However, under our test conditions (under Ar), Ni catalytic effect can only impact oxygen dissociation (air rich side) of recombination (air poor side). The most important impact is the increase of the exchange surface due to the porous layers.

The  $\text{La}_{0.8}\text{Sr}_{0.2}\text{Fe}_{0.7}\text{Ga}_{0.3}\text{O}_{3-\delta}$  porous layer is deposited by screen printing of an ink containing 60 vol% of 5  $\mu\text{m}$  diameter rice starch particles. After co-sintering at 1100 °C during 30 min of the thick dense and thin porous layer, the porosity is fully interconnected with an average diameter around 4  $\mu\text{m}$ , and a volume fraction close to 50%.

The porosity of LSFN catalyst layers elaborated with the same ink and sintering conditions (1100 °C during 30 min, 60 vol% of rice starch) vary from 27 to 50 vol%. The microstructure of the catalyst layers includes many interconnected pore with an average diameter around 4  $\mu\text{m}$  compared to 0.2  $\mu\text{m}$  without pore forming agent. Large interconnections are necessary to facilitate gas flow through the porous layer (Fig. 9).

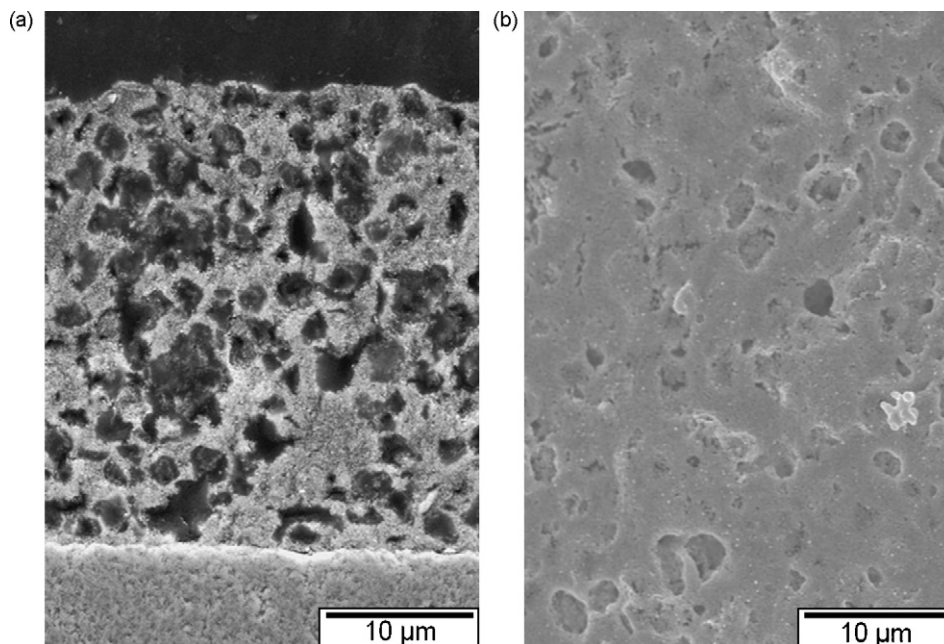


Fig. 9. SEM micrographs of p LSFN/LSFG<sub>8273</sub> polished cross section (a) highly porous (50%)  $\text{La}_{0.8}\text{Sr}_{0.2}\text{Fe}_{0.7}\text{Ni}_{0.3}\text{O}_{3-\delta}$  coating on  $\text{La}_{0.8}\text{Sr}_{0.2}\text{Fe}_{0.7}\text{Ga}_{0.3}\text{O}_{3-\delta}$  membrane (b) top view of porous  $\text{La}_{0.8}\text{Sr}_{0.2}\text{Fe}_{0.7}\text{Ni}_{0.3}\text{O}_{3-\delta}$ .

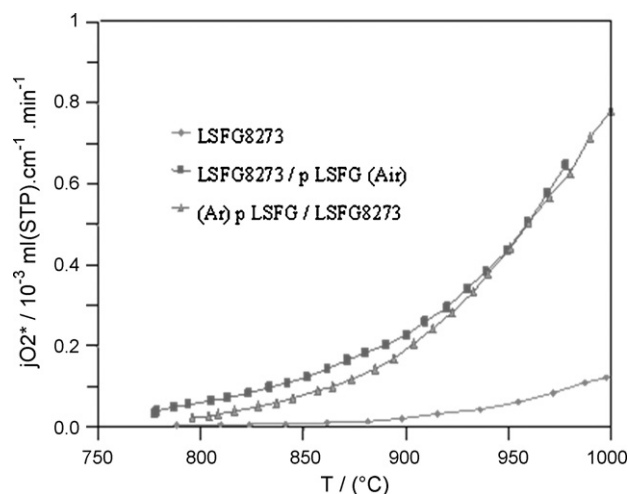


Fig. 10. Specific oxygen semi-permeation flux of  $\text{La}_{0.8}\text{Sr}_{0.2}\text{Fe}_{0.7}\text{Ga}_{0.3}\text{O}_{3-\delta}$  with a porous coating (p) of  $\text{La}_{0.8}\text{Sr}_{0.2}\text{Fe}_{0.7}\text{Ga}_{0.3}\text{O}_{3-\delta}$  on oxidizing and reducing face compared to of  $\text{La}_{0.8}\text{Sr}_{0.2}\text{Fe}_{0.7}\text{Ga}_{0.3}\text{O}_{3-\delta}$  membrane without coating?

The LSFG<sub>8273</sub>/p LSFG (air) and (Ar) p LSFG/LSFG<sub>8273</sub> consist in 1 mm thick  $\text{La}_{0.8}\text{Sr}_{0.2}\text{Fe}_{0.7}\text{Ga}_{0.3}\text{O}_{3-\delta}$  dense membrane coated by a 20–25 μm thick  $\text{La}_{0.8}\text{Sr}_{0.2}\text{Fe}_{0.7}\text{Ga}_{0.3}\text{O}_{3-\delta}$  porous layer respectively on oxygen rich and oxygen poor sides.

Fig. 10 shows the influence of a  $\text{La}_{0.8}\text{Sr}_{0.2}\text{Fe}_{0.7}\text{Ga}_{0.3}\text{O}_{3-\delta}$  porous layer on oxygen poor or oxygen rich side of  $\text{La}_{0.8}\text{Sr}_{0.2}\text{Fe}_{0.7}\text{Ga}_{0.3}\text{O}_{3-\delta}$  membrane. The oxygen flux increases with the increase to the exchange surface developed, by the porosity of the  $\text{La}_{0.8}\text{Sr}_{0.2}\text{Fe}_{0.7}\text{Ga}_{0.3}\text{O}_{3-\delta}$  porous layers, on both sides. For instance at 900 °C, the specific oxygen flux is 0.27 ml cm<sup>-1</sup> min<sup>-1</sup> for  $\text{La}_{0.8}\text{Sr}_{0.2}\text{Fe}_{0.7}\text{Ga}_{0.3}\text{O}_{3-\delta}$  dense membrane and 2 ml cm<sup>-1</sup> min<sup>-1</sup> for LSFG<sub>8273</sub>/p LSFG (air). Besides, Table 3 shows that the apparent activation energies for oxygen permeation decrease slightly with the increase of the exchange surface, although these values of apparent activation energies present likely a large incertitude. This assumes that the oxygen transport through the LSFG membranes is governed by surface exchanges kinetics.

Further improvement can be expected using materials having better surface exchange kinetic than Ga-containing perovskite. For example, Ni-containing materials, could be advantageously used on the oxygen poor side of the membrane especially for methane conversion applications [25,26].

In this respect, a catalytic layer of  $\text{La}_{0.8}\text{Sr}_{0.2}\text{Fe}_{0.7}\text{Ni}_{0.3}\text{O}_{3-\delta}$  was coated onto the oxygen poor side (Fig. 2), referenced p LSFN/LSFG<sub>8273</sub>. Ni is introduced in the perovskite structure for its high catalytic activity for methane conversion reactions. At 900 °C, under an air/argon gradient, the specific oxygen flux is increasing from  $2.7 \times 10^{-5}$  ml cm<sup>-1</sup> min<sup>-1</sup> for

Table 3  
Apparent activation energies for oxygen permeation of membranes.

Membranes	Apparent activation energies
LSFG <sub>8273</sub>	190–220 kJ/mol
LSFG <sub>8273</sub> /p LSFG (air)	150–170 kJ/mol
(Ar) p LSFG/LSFG <sub>8273</sub>	160–190 kJ/mol

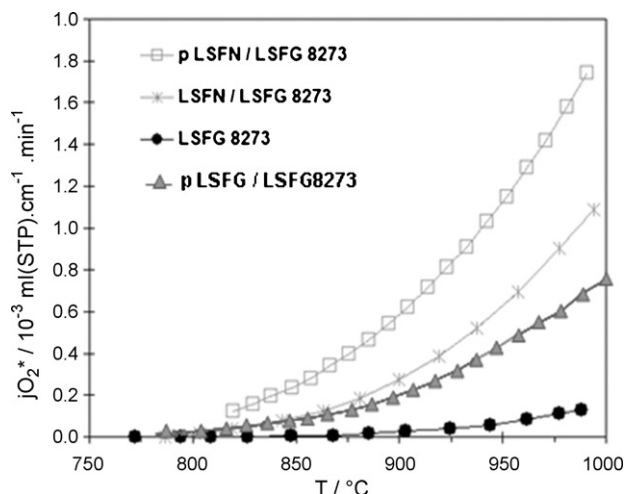


Fig. 11. Specific oxygen semi-permeation flux through  $\text{La}_{0.8}\text{Sr}_{0.2}\text{Fe}_{0.7}\text{Ga}_{0.3}\text{O}_{3-\delta}$  with and without coating of  $\text{La}_{0.8}\text{Sr}_{0.2}\text{Fe}_{0.7}\text{Ni}_{0.3}\text{O}_{3-\delta}$  on the air poor side.

Table 4  
Apparent activation energies for oxygen semi-permeation of membranes.

Membranes	Apparent activation energies
LSFG <sub>8273</sub>	190–220 kJ/mol
p LSFG/LSFG <sub>8273</sub>	160–190 kJ/mol
LSFN/LSFG <sub>8273</sub>	170–200 kJ/mol
p LSFN/LSFG <sub>8273</sub>	160–190 kJ/mol

LSFG<sub>8273</sub> to  $6.3 \times 10^{-4}$  ml cm<sup>-1</sup> min<sup>-1</sup> for p LSFN/LSFG<sub>8273</sub>. As a comparison, the flux is  $2.0 \times 10^{-4}$  ml cm<sup>-1</sup> min<sup>-1</sup> for p LSFG/LSFG<sub>8273</sub>. The higher developed surface on the air poor side of the membrane, and/or the catalyst effect of the Ni-containing material, have a more important effect on the oxygen flux than on the oxygen rich side.

The surface exchange kinetic is likely larger on the oxygen poor side with a  $\text{La}_{0.8}\text{Sr}_{0.2}\text{Fe}_{0.7}\text{Ni}_{0.3}\text{O}_{3-\delta}$  coating than on the oxygen rich side with  $\text{La}_{0.8}\text{Sr}_{0.2}\text{Fe}_{0.7}\text{Ga}_{0.3}\text{O}_{3-\delta}$  coating. The limiting step is the surface exchange on the oxygen rich side. Further improvement could be reached by coating both sides of the membrane with a porous layer.

As shown in Fig. 11, at 900 °C, the specific oxygen semi-permeation flux is  $2.8 \times 10^{-4}$  ml cm<sup>-1</sup> min<sup>-1</sup> for LSFN/LSFG<sub>8273</sub> (27 vol% of porosity) membrane, two times lower than for a p LSFN/LSFG<sub>8273</sub> (50 vol% of porosity) membrane. The porosity of the layer has also an impact on the oxygen flux. Low porosity (27 vol%) leads to smaller oxygen flux than a 50 vol% porous layer. However, the Ni-containing formulations seem to have no significant effect on the activation energy for oxygen permeation (Table 4) of which the values present a large incertitude.

The results obtained are in good agreement with previous published works from Lee et al. [27] for  $\text{La}_{0.7}\text{Sr}_{0.3}\text{Fe}_{0.6}\text{Ga}_{0.4}\text{O}_{3-\delta}$  coated with a  $\text{La}_{0.8}\text{Sr}_{0.2}\text{CoO}_{3-\delta}$  layer and Etchegoyen et al. [28] for  $\text{La}_{0.6}\text{Sr}_{0.4}\text{Fe}_{0.9}\text{Ga}_{0.1}\text{O}_{3-\delta}$  coated with  $\text{La}_{0.6}\text{Sr}_{0.4}\text{Co}_{0.8}\text{Fe}_{0.2}\text{O}_{3-\delta}$ .

#### 4. Conclusions

$\text{La}_{0.8}\text{Sr}_{0.2}\text{Fe}_{0.7}\text{Ga}_{0.3}\text{O}_{3-\delta}$  perovskite exhibits a good compromise in terms of dimensional, chemical and structural stabilities for methane conversion applications. Under air and argon atmospheres, a reversible structural phase transition from monoclinic to rhomboedral was observed around 300 °C.

Oxygen flux measurements through several microstructures and architectures of membranes have shown that surface exchange kinetic is the limiting step. By the way, it was not possible to evaluate the impact of the grain size.

Porous layers have been coated on the oxygen rich side or on the oxygen poor side of the membrane. Oxygen flux increases with the development of the surface and/or the catalytic effect of the material on oxygen dissociation or recombination. The total volume of the porosity has also an impact on the flux. There should be an optimum enabling the access of the gas to the membrane and developing enough surfaces. Then, better oxygen fluxes are expected by coating both sides of the membrane with porous layers of dedicated formulations.

#### Acknowledgements

The authors would like to thank Air Liquide for technical and financial support and ADEME (French environment and energy management agency) for financial support of this Study.

#### References

- [1]. Rostrup-Nielsen JR. Syngas in perspective. *Catal Today* 2002;**71**(3–4): 243–7.
- [2]. Teraoka Y, Zhang H-M, Furukawa S, Yamazoe N. Oxygen permeation through perovskite-type oxides. *Chem Lett* 1985;1743–86.
- [3]. Bouwmeester HJM, Burggraaf AJ. Dense ceramic membranes for oxygen separation. *Fundam Inorg Membr Sci Technol* 1996.
- [4]. Sammells AF, Schwartz M, Mackay RA, Barton TF, Peterson DR. Catalytic membrane reactors for spontaneous synthesis gas production. *Catal Today* 2000;**56**(1–3):325–8.
- [5]. Wilhelm DJ, Simbeck DR, Karp AD, Dickenson RL. Syngas production for gas-to-liquids applications: technologies, issues and outlook. *Fuel Process Technol* 2001;**71**(1–3):139–48.
- [6]. Juste E, Julian A, Etchegoyen G, Geffroy PM, Chartier T, Richet N, Del Gallo P. Oxygen permeation, thermal and chemical expansion of  $(\text{La}, \text{Sr})(\text{Fe}, \text{Ga})\text{O}_{3-\delta}$  perovskite membranes. *J Membr Sci* 2008;**319**(1–2):185–91.
- [7]. Kharton VV, Yaremchenko AA, Patrakeev MV, Naumovich EN. Thermal and chemical induced expansion of  $\text{La}_{0.3}\text{Sr}_{0.7}(\text{Fe}, \text{Ga})\text{O}_{3-\delta}$  ceramics. *J Eur Ceram Soc* 2003;**23**(9):1417–26.
- [8]. Julian A, Juste E, Geffroy P-M, Tessier-Doyen N, Del Gallo P, Richet N, Chartier T. Thermal behaviour of  $\text{La}_{0.8}\text{Sr}_{0.2}\text{Fe}_{1-x}\text{Ga}_x\text{O}_{3-\delta}$  ( $x=0$  or  $x=0.3$ ). *J Eur Ceram Soc* 2009;**29**(12):2603–10.
- [9]. Koutcheiko S, Whitfield P, Davidson I. Electrical and thermal properties of  $\text{La}_{0.7}\text{Sr}_{0.3}\text{Ga}_{0.6}\text{Fe}_{0.4}\text{O}_3$  ceramics. *Ceram Int* 2006;**32**(3):339–44.
- [10]. McIntosh S, Vente JF, Haije WG, Blank DHA, Bouwmeester HJM. Structure and oxygen stoichiometry of  $\text{SrCo}_{0.8}\text{Fe}_{0.2}\text{O}_{3-\delta}$  and  $\text{Ba}_{0.5}\text{Sr}_{0.5}\text{Co}_{0.8}\text{Fe}_{0.2}\text{O}_{3-\delta}$ . *Solid State Ionics* 2006;**177**(19–25):1737–42.
- [11]. Wang H, Tablet C, Yang W, Caro J. In situ high temperature X-ray diffraction studies of mixed ionic and electronic conducting perovskite-type membranes. *Mater Lett* 2005;**59**(28):3750–5.
- [12]. Etchegoyen G, Chartier T, Julian A, Del-Gallo P. Microstructure and oxygen permeability of a  $\text{La}_{0.6}\text{Sr}_{0.4}\text{Fe}_{0.9}\text{Ga}_{0.1}\text{O}_{3-\delta}$  membrane containing magnesia as dispersed second phase particles. *J Membr Sci* 2006;**268**(1):86–95.
- [13]. Kharton VV, Marques FMB. Mixed ionic-electronic conductors: effects of ceramic microstructure on transport properties. *Curr Opin Solid State Mater Sci* 2002;**6**(3):261–9.
- [14]. Kharton VV, Tikhonovich VN, Shuangbao L, Naumovich EN, Kovalevsky AV, Viskup AP, Bashmakov IA, Yaremchenko AA. Ceramic microstructure and oxygen permeability of  $\text{SrCo}(\text{Fe}, \text{M})\text{O}_{3-\delta}$  ( $\text{M} = \text{Cu}$  or  $\text{Cr}$ ) perovskite membranes. *J Electrochem Soc* 1998;**145**:1363.
- [15]. Wang H, Tablet C, Feldhoff A, Caro J. Investigation of phase structure, sintering, and permeability of perovskite-type  $\text{Ba}_{0.5}\text{Sr}_{0.5}\text{Co}_{0.8}\text{Fe}_{0.2}\text{O}_{3-\delta}$  membranes. *J Membr Sci* 2005;**262**(1–2):20–6.
- [16]. Martynczuk J, Arnold M, Feldhoff A. Influence of grain size on the oxygen permeation performance of perovskite-type  $(\text{Ba}_{0.5}\text{Sr}_{0.5})(\text{Fe}_{0.8}\text{Zn}_{0.2})\text{O}_{3-\delta}$  membranes. *J Membr Sci* 2008;**322**(2):375–82.
- [17]. Arnold M, Martynczuk J, Efimov K, Wang H, Feldhoff A. Grain boundaries as barrier for oxygen transport in perovskite-type membranes. *J Membr Sci* 2008;**316**(1–2):137–44.
- [18]. Kharton VV, Naumovich EN, Kovalevsky AV, Viskup AP. Mixed electronic and ionic conductivity of  $\text{LaCo}(\text{M})\text{O}_3$  ( $\text{M} = \text{Ga}, \text{Cr}, \text{Fe}$  or  $\text{Ni}$ ). IV. Effect of preparation method on oxygen transport in  $\text{LaCoO}_{3-\delta}$ . *Solid State Ionics* 2000;**138**(1–2):135–48.
- [19]. Diethelm S, Van herle J, Sfeir J, Buffat P. Correlation between oxygen transport properties and microstructure in  $\text{La}_{0.5}\text{Sr}_{0.5}\text{FeO}_{3-\delta}$ . *J Eur Ceram Soc* 2005;**25**(12):2191–6.
- [20]. Lin YS, Wang W, Han J. Oxygen permeation through thin mixed-conducting solid oxide membranes. *AIChE J* 1994;**40**(5):786.
- [21]. Chen CH, Bouwmeester HJM, Van Doorn RHE, Kruidhof H, Burggraaf AJ. Oxygen permeation of  $\text{La}_{0.3}\text{Sr}_{0.7}\text{CoO}_{3-\delta}$ . *Solid State Ionics* 1997;**98**(1–2):7–13.
- [22]. Gellings PJ, Bouwmeester HJM. Ion and mixed conducting oxides as catalysts. *Catal Today* 1992;**12**(1):1–105.
- [23]. Sunarso J, Baumann S, Serra JM, Meulenberg WA, Liu S, Diniz Da Costa JC. Mixed ionic-electronic conducting (MIEC) ceramic-based membranes for oxygen separation. *J Membr Sci* 2008;**320**(1–2):13–41.
- [24]. Julian A, Juste E, Geffroy P-M, Coudert V, Richet N, Chartier T, Del Gallo P. Elaboration of  $\text{La}_{0.8}\text{Sr}_{0.2}\text{Fe}_{0.7}\text{Ga}_{0.3}\text{O}_{3-\delta}/\text{La}_{0.8}\text{M}_{0.2}\text{FeO}_{3-\delta}$  ( $\text{M} = \text{Ca}, \text{Sr}$  and  $\text{Ba}$ ) asymmetric membranes by tape-casting and co-firing. *J Membr Sci* 2009;**333**(1–2):132–40.
- [25]. Pompeo F, Nichio NN, Ferretti OA, Resasco D. Study of Ni catalysts on different supports to obtain synthesis gas. *Int J Hydrogen Energy* 2005;**30**(13–14):1399–405.
- [26]. Chu Y, Li S, Lin J, Gu J, Yang Y. Partial oxidation of methane to carbon monoxide and hydrogen over  $\text{NiO}/\text{La}_2\text{O}_3/\gamma\text{-Al}_2\text{O}_3$  catalyst. *Appl Catal A: Gen* 1996;**134**(1):67–80.
- [27]. Lee KS, Lee S, Kim JWK, Woo S. Enhancement of oxygen permeation by  $\text{La}_{0.6}\text{Sr}_{0.4}\text{CoO}_{3-\delta}$  coating in  $\text{La}_{0.7}\text{Sr}_{0.3}\text{Ga}_{0.6}\text{Fe}_{0.4}\text{O}_{3-\delta}$  membrane. *Desalination* 2002;**147**(1–3):439–44.
- [28]. Etchegoyen G, Chartier T, Del-Gallo P. An architectural approach to the oxygen permeability of a  $\text{La}_{0.6}\text{Sr}_{0.4}\text{Fe}_{0.9}\text{Ga}_{0.1}\text{O}_{3-\delta}$  perovskite membrane. *J Eur Ceram Soc* 2006;**26**(13):2807–15.